TSV Antennas for Multi-Band Wireless Communication

Vasil Pano, *Member IEEE,* Ibrahim Tekin, *Senior Member IEEE,*
Isikcan Yilmaz, *Student Member IEEE,* Yuqiao Liu, *Student Member IEEE,*
Kapil Dandekar, *Senior Member IEEE,* and Baris Taskin, *Senior Member IEEE*

***Abstract*—On-chip wireless links offer improved network performance due to long distance communication, additional bandwidth, and broadcasting capabilities of antennas. This work challenges the on-chip antenna design conventions, and pushes toward a Through-Silicon Via-based antenna design called TSV_A that establishes multi-band wireless communication through the silicon substrate medium with only a 3 dB loss over a 30mm on-chip distance. The TSV_A performance is evaluated in both Finite Element Method and system-level Network-on-Chip (NoC) simulations. A comparison to traditional wire-based NoCs, analysis of wireless multi-bands, and technology scaling to demonstrate the substantial area improvements compared to traditional wireless NoCs (up to 99.88%) are performed. Simulation results show an improvement in network latency up to ∼13% (average improvement of ∼7%), energy-delay improvements of ∼34% on average, and an improvement in throughput up to ∼34% (average improvement of ∼23%), using Wireless NoC with multi-band TSV_As. The improved signal performance of TSV_A, and multi-band capabilities, are ideal for wireless intercell communication for programmable metasurfaces with dedicated communication layers.**

***Index Terms*—network-on-chip, on-chip antenna, wireless interconnect, multi-band, tsv**

I. Introduction

On-chip antennas, implementing wireless interconnects, are introduced for improved scalability of NoCs in [1–3]. These antennas act as shortcut links for on-chip long-distance communication. On-chip antennas offer improved latency and broadcasting capabilities. Most antennae in literature operate on a single wireless channel based on the resonant frequency, which limits the overall in-flight transactions on the network. Additional wireless channels in the network would require an antenna with multiple resonant frequencies, and added modulation in order to facilitate flow control and prevent interference.

This material is based upon work supported by the National Science Foundation under Grant No. 1305350.

Vasil Pano, Yuqiao Liu, Kapil Dandekar, and Baris Taskin are with the Electrical and Computer Engineering Department, Drexel University, Philadelphia, PA 19104 USA (email: vasilpano@gmail.com and taskin@coe.drexel.edu)

Ibrahim Tekin is with Electronics Engineering, Sabanci University, Istanbul, Turkey (email: tekin@sabanciuniv.edu)

Isikcan Yilmaz is with Apple Inc. in Culver City, California, USA (email: can158@gmail.com)

©©20xx IEEE. Personal use of this material is permitted. Permission from IEEE must be obtained for all other uses, including reprinting/republishing this material for advertising or promotional purposes, collecting new collected works for resale or redistribution to servers or lists, or reuse of any copyrighted component of this work in other works.

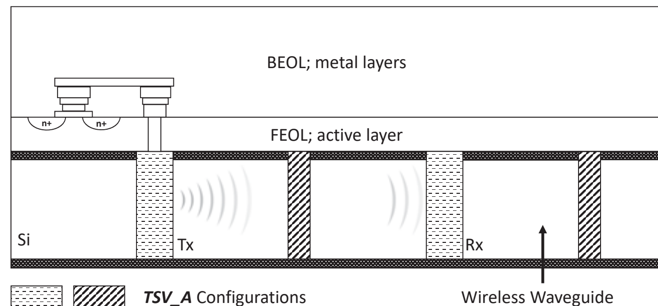

Fig. 1. Die cross-section with 4 TSV_As for on-chip wireless communication.

Multiple wireless bands (channels) can be achieved in various ways; each at a unique cost of area, power, and complexity. The established methods to have more than one wireless band include: 1) Directional antennas, 2) splitting the transmission bandwidth of the antenna, and 3) include different types of antennas at different resonant frequencies. Directional antennas [4, 5], which work in pairs, allow for multiple wireless channels but their functionality is based on line-of-sight and is subject to cross-interference. Creating multiple wireless channels by splitting the bandwidth of the antenna requires more complex modulation logic and additionally the specified antenna must achieve a high enough bandwidth. Antennas with different resonant frequencies can be implemented, although the fabrication process will increase in complexity due to the all the possible antenna designs (dipole, zig-zag, meander, folded, log-periodic). Due to the limiting surface propagation of the wave and the lack of any waveguides, path loss increases exponentially with distance until the antenna cannot be operational at the target maximum distance of the transceiver. Adding multiple antennas to account for path loss is prohibitive due to a significant design overhead.

This work proposes a novel on-chip antenna (TSV_A) implemented with TSVs based on the disc-loaded monopole antenna-style. The proposed antenna design can operate long-distance (up to 30mm is simulated with only 3 dB loss) and can be optimized to support multiple frequency bands without needing line-of-sight. An illustrative cross-section of two TSV_A pairs is shown in Figure 1. The cross-section includes both the front and back end of line (FEOL and BEOL) of standard CMOS fabrication to visualize the location of the main propagation wave (in the Si layer) and the TSV_A.

Finite-element method through High Frequency Structure Simulator (HFSS) and printed circuit board (PCB) prototyping are used to validate operation of the TSV_A. A custom mapping algorithm, which considers the multi-band properties of the TSV_A, is introduced to improve the placement location on the NoC. Wireless Network-on-Chip (WNoC) evaluations utilizing a cycle-accurate SystemC network simulator are performed to measure performance improvement between to wireless and non-wireless topologies.

A. TSV_A Metasurface Intercell Wireless Communication

In recent years, on-chip monopole antennae similar to TSV_A, have been investigated as a viable alternative to transmit commands for software-defined metasurfaces [6–10]. Metamaterials and metasurfaces are artificial materials with programmable unit cell structures to achieve versatile functionalities. Communication between these unit cells and the controllers that "re-program" them is especially important in enabling metasurface reconfigurability. Wireless communication between unit cells alleviates some of the issues that wired communication encounters, including layout routing with the increase in size of the metasurface [8]. With the increasing adoption of metamaterials and metasurfaces, there is a need for reliable antenna capable of distributing commands across all unit cells for metasurface reconfigurability.

TSV_A is the ideal candidate for improved wireless communication within a metasurface, with the ability to transmit at long distances with minimal loss. Support for multi-band operation of TSV_As allow for separate commands to be issued at different unit cells of a metasurface at the same time, improving the operation of the software-defined metasurface considerably. Although TSV_A is primarily designed for on-chip wireless communication, the ability to increase the size of the proposed antenna is effectively and accurately demonstrated with the larger PCB prototype detailed in this work.

An overview of the related works is presented in Section II. The proposed TSV_A is detailed in Section III. FEM evaluation of the proposed antenna and the multi-band operation are presented in Section IV. An in-depth NoC analysis with the TSV_A integration is performed in Section V. Finally, the conclusions of this work are outlined in Section VI.

II. Related Works

The authors' recent work [11, 12] introduced the feasibility of the TSV Antenna within a single band and compared the performance of a TSV_A antenna to other state of the art antennae. In [12], a PCB prototype is fabricated and measured with a VNA in order to verify functionality and performance. PCB measurements results indicate that the TSV_A is capable of transmission up to 800mil (20mm) distance with only 5 dB to 10 dB insertion loss. Multiple TSV_A structures with additional via to improve directivity are measured and evaluated, improving insertion loss from the standalone TSV_A. Finite element method simulations, executed through HFSS, appear to match the measured results in lower frequencies. The study of the multi-band properties of TSV_A and system-level Wireless Network-on-Chip evaluation, both of which are detailed in this paper, were not performed in prior works. Multi-band operation makes multiple wireless channels feasible, such as those necessary in the application highlighted in Section I-A, programming of metasurface unit cells through multiple wireless channels.

The feasibility of on-chip wireless interconnects is first studied by K. Kim and Kenneth K.O. [1]. Subsequent work by Floyd and Lin [13, 14] demonstrate multiple fabricated (90nm–130nm technology) antennas to be fully operational. Carbon nanotube (CNT) as the primary material for dipole antennas is proposed in [15]. The distinct properties of CNT support operational in the THz or optical frequency range and can achieve a bandwidth of $\sim$500 GHz. Although this technology is promising, fabrication is challenging.

The addition of wireless interconnects in NoCs has been studied extensively. The work on WNoCs focuses on the key elements necessary for wireless operation, including topology, routing, flit/packet wireless transmission, and various wireless protocols. For example, Pande and Ganguly [16, 17] introduce WNoC utilizing the theoretical feasibility of CNTs in [15]. Abadal et al. [18, 19] have studied opportunistic beamforming in wireless network-on-chip and built a reconfigurable beamforming scheme and have achieved moderate gains and beamwidths below 90°.

Yu et al. [20, 21] propose (and fabricated in 65nm bulk CMOS process) an on-off keying (OOK) transmitter and receiver which consume only 1.2 pJ/bit at a data rate of 16 Gb/s operating at 60 GHz. The energy per bit, area values, and maximum operation distance (20mm) of the wireless transceiver from Yu et al. [20, 21] are utilized in the system-performance results reported in this work.

RF-interconnects, proposed in [22, 23] utilize transmission lines (on or off chip) to guide EM waves from the transmitter to the receiver. RF-I multi-band properties (each transmission line can be a separate band) show a clear distinction from the single wireless channel operation. Although capable of total aggregate data rate of 30 Gb/s per RF-I wire, the wireless benefits of broadcast and non-line-of-sight (NLOS) are not possible in RF-I interconnects.

Mondal et al. [4] and Mineo et al. [5] evaluate WNoCs with multi-band by utilizing the directional characteristics of on-chip antennas. Mondal et al. utilize a planar log-periodic antenna with enhanced directional capabilities to form three concurrent wireless links. Each pair of antennas do not have line-of-sight with the rest, therefore interference is avoided. The planar log-periodic antennas occupy a large chip area and is interference-free only if the antenna pairs do not cross. Mineo et al. utilize a zig-zag antenna at different angles to form groups of wireless communication within a single chip. Similar issues to Mondal et al. resurface, antennas have to be aligned a specific position and interference is only avoided if there is no line-of-sight between groups.

More et al. [24] evaluate the impact of antenna positioning on the different metal layers of the BEOL stack. It is observed that the carrier frequency of a meander antenna [25, 26] shifts if it is placed in metal layer 5 as opposed to metal layer 10. The feasibility of WNoCs with multi-band by placing multiple meander antennas at different metal layers is studied. The

conclusions indicate that it is possible to create multi-bands without line-of-sight but the transmission loss is too large and no system-level evaluations are performed. The meander and planar log-periodic antennas are evaluated against the proposed TSV_A.

A Through-Glass Via monopole antenna for 3D IC is proposed in [27, 28]. HFSS simulations and PCB fabrication show a carrier frequency between 70 to 90 GHz, with a bandwidth of ∼10 GHz. The fabricated TGV antenna is designed at 6 GHz and displays similar characteristics to the simulated version. NoC performance and path loss are not evaluated for TGVs, therefore system-level performance impacts are unknown.

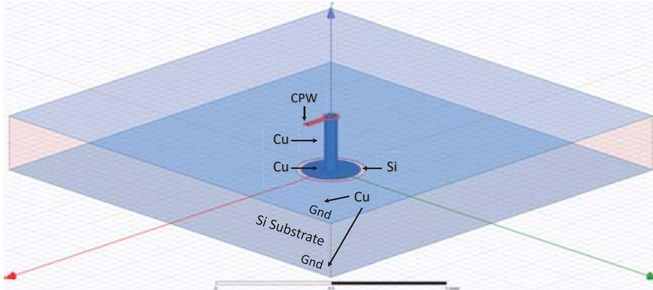

(a) HFSS Simulation Environment (Scale 0-1mm)

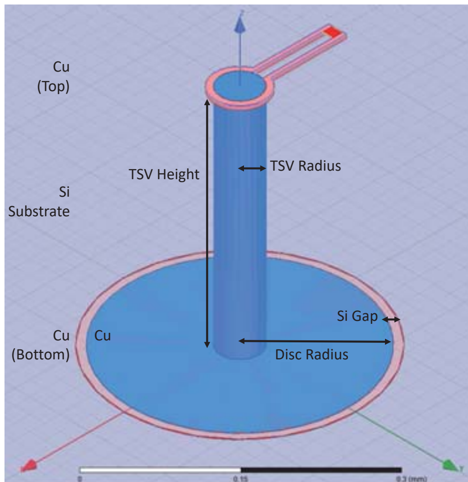

(b) Close-up of TSV_A (Scale 0-0.3mm)

Fig. 2. HFSS Design of TSV_A.

III. TSV Antenna for Multi-Band Operation

The design of a TSV_A [12] is based on a typical disc-loaded monopole antenna. The detailed model of the TSV_A from [12] is shown in Figure 2. A small gap is etched around the TSV in the bottom ground plane to modify the capacitance of the structure. This cylindrical disc can be used for impedance matching to improve the overall signal strength. Top and bottom ground planes (1μm thickness each in the simulated environment) are added to the silicon substrate in the FEOL of IC fabrication to strengthen the act of the silicon substrate layer as a wireless waveguide for the signal. The TSV_A, as proposed in this paper, is amenable for operation in multiple bands of frequency, based on the different design parameters of the TSV. The height and the radius of a TSV are the main design parameters of the TSV_A. The ground plane, the disc radius, and the Si gap radius are additional design parameters of the TSV_A.

The TSV_A is placed inside the layer of silicon (Si) substrate. The size of the silicon box is 3mm × 3mm × *TSV height* (one of the tunable parameters of the TSV_A). The relative dielectric constant (ε_r) used for the Si substrate is 11.7. The TSV material, top, and bottom ground planes are selected to be copper (Cu).

A coplanar waveguide (CPW) is used to feed the signal to the TSV_A. The CPW is only feeding antenna, and does not impact the resonant frequency of the antenna. Current traverses in from the signal line of the CPW and then travels along the via and radially outwards from the bottom disk. The radiating part of the antenna is the via part; However, both the via and the disk determine the resonance frequency of the antenna.

The resonance length of the antenna is comprised of both the TSV height and the disc radius. For a 60 GHz monopole antenna on air, the wavelength is 5mm, and the $\lambda/4$ = 1.25mm. Silicon of relative dielectric constant of 11.7 further decreases the resonant length to 365 μm. The antenna size (TSV height + disc radius – via radius) is smaller that this resonant length as the disc edge and the ground plane form a capacitor. The value of this capacitance can be adjusted by varying the Si gap size. Due to skin effect, the current will flow on the skin of the conductors. As the TSV radius is increased, the current path is shorter, therefore it is a shorter antenna and the resonance frequency increases. Additionally, as the TSV radius is decreased, the path that the current flows is increased and hence the resonant frequency decreases. Resonant frequency is designed with these design parameters, e.g. with the silicon in the gap, and the capacitance.

A. *TSV Manufacturing Feasibility*

The feasibility of the aspect ratio of 5:1 selected in this work for the largest TSV_A size is demonstrated in [29–32]. An even wider range of via holes, up to an aspect ratio of 100:5, are possible, for example in DRIE [30]. In addition, the research community has investigated the process robustness in-depth, sweeping the via dimensions from 3-80 μm wide and 45-160 μm deep in in 150mm and 200mm wafers [29]. There is active research in the manufacturing of TSVs for 3D ICs and interposers. Small dimension changes for crosstalk avoidance, driving strength, stress, vertical reach and thermal conductivity are studied in [29, 33, 34]. The TSV_As benefit from these packaging and manufacturing innovations. The configuration of the bands can be advanced as the aspect ratio of TSVs improve through this active area of research.

Further work on process variation and sensitivity is required for the successful integration of TSV_As with multi-band support. The same thoroughness must be dedicated by manufacturing experts to investigate the robustness of a wide range of TSVs to be used as TSV_As. Any and all manufacturing limitations can be modeled as design guidelines for TSV_As, and routinely updated with each advancement in manufacturing improvements of TSVs (and consequently, TSV_As). The goal of this work is to demonstrate the design

space with the known TSV_A manufacturing limitations. The number of available bands will increase as the manufacturing process for TSVs and interposers mature. A thorough robustness investigation will determine i) the subset of TSV_As capable of interference-free wireless transmission, and ii) a set of design rules to help architects and manufacturers finely tune each TSV_A and wireless band.

IV. Simulation Study of TSV_A

HFSS simulation results for the TSV_A are provided in Section IV-A to verify: 1) Communication quality through scattering parameters, and, 2) bandwidth analysis to demonstrate feasibility of multi-band operation. Cross-talk analysis of two pairs of TSV_As is performed in Section IV-B. Evaluation of the TSV_A without the bottom ground plane is performed in Section IV-C. TSV_A design space exploration of possible configurations are evaluated in Section IV-D. Path loss analysis is presented in Section IV-E. Analyses of the interference between TSV_As, including those with TSVs, are presented in Section IV-F.

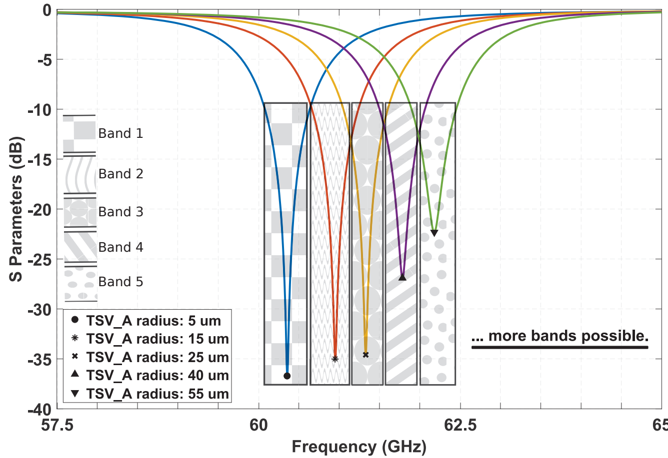

Fig. 3. Reflection coefficient (S11) versus frequency. Variable TSV radius. Each box represents a separate band. (HFSS Simulated Results)

A. TSV_A Scattering Parameters

S-parameters describe the input-output relationship between antennas, characterizing the channel to identify the frequency and bandwidth of transmission. Reflection coefficient (S11) represents how much power is reflected from the TSV_A (lower is better). The TSV_A reflection coefficients for (arbitrarily selected) 5 representative bands are shown in Figure 3, and there is room for more bands, as marked on the figure. With the change in radius, the resonant frequency shifts, with non-overlapping bands with viable bandwidth of communication. Other TSV_As with different design parameters (height, radius and optionally bottom plane disc radius and Si gap dimension in Figure 2(b)) can be implemented on-chip at design-time to enable multi-band transmission. The radiation pattern of a single TSV_A is shown in Figure 4 and Figure 5. As it can be seen, TSV_A has an omni-directional radiation pattern.

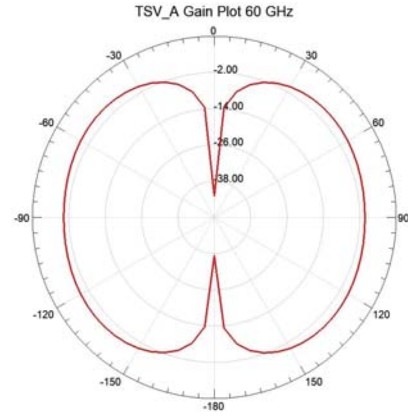

Fig. 4. Radiation Pattern of TSV_A at 60 GHz. (HFSS Simulated Results)

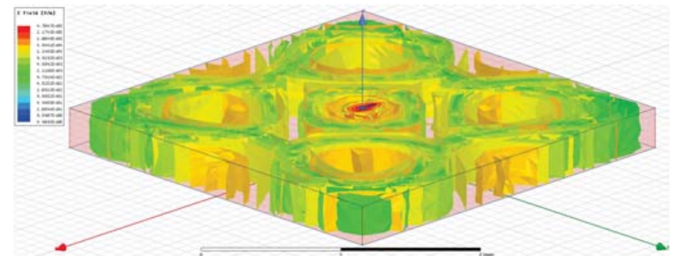

Fig. 5. Radiation Pattern in the Silicon Substrate at 60 GHz (Scale 0-2mm). (HFSS Simulated Results)

B. TSV_A Cross-Talk

In Figure 6, two different pairs of TSV_As are placed on the same board at a distance of 6mm for each pair. The TSV_A pairs have two different radii. `TSV_A 1` and `TSV_A 2` have a radius of 20μm and `TSV_A 3` and `TSV_A 4` have a radius of 100μm. These two pairs have distinct resonant frequencies that do not interfere with each-other. S-parameters for both pairs are shown in Figure 7. Both TSV_A dimensions have approximately the same bandwidth and transmission coefficient (S21, S43). It is observed from Figure 7 that the two pairs of TSV_As do not interfere with each-other during transmission and are adequately spaced to filter two distinct structures. Although the transmission coeff. between `TSV_A 1` and `TSV_A 3` is ∼-10 dB, cross-talk is not an issue due to the different resonant frequencies of both TSV_As and the gap in transmission coeff. between S31 and S21 (-10 dB vs -3 dB). Therefore, frequency filtering (through a typical bandpass filter) can be applied to distinguish the receiving signal from noise.

$$\begin{gathered}\Delta = \frac{500\ MHz}{600\ GHz} = \frac{0.5}{60} = 0.008 \\ W_0 = 60GHz, W = 60.5GHz \\ W_c = \frac{1}{0.008} * (\frac{60.5}{60} - \frac{60}{60.5}) = 2\end{gathered} \tag{1}$$

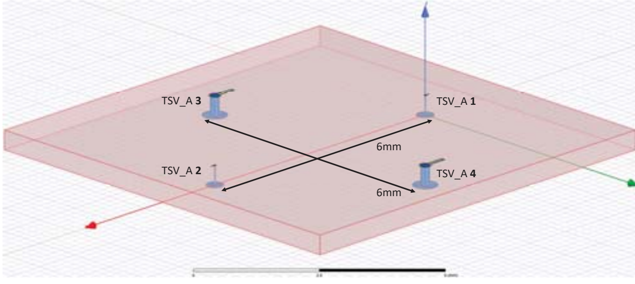

Fig. 6. Two pairs of TSV_As with two different radii (20μm and 100μm) placed at 6mm distance. (Scale 0-5mm)

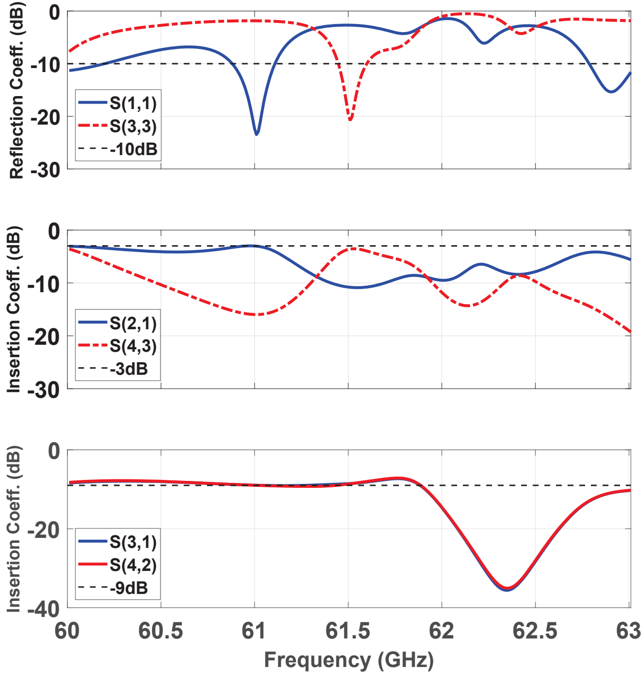

Fig. 7. S-parameters for two pairs of TSV_As at two different radii placed at 6mm distance. (HFSS Simulated Results)

A bandpass filter can be designed at 60 GHz with 500 MHz (59.75-60.25 Ghz) bandwidth. The bandpass filter is made of 2 inductors and capacitors [35]. In addition, the research community has investigated bandpass filter solutions [36, 37] to obtain 25 dB attenuation at 60.5 Ghz with an order of 2 as shown in Equation 1.

An alternative solution to band-pass filtering is the use of tunable transceivers. For instance, the transceiver proposed in Yu et al [20] is tunable to operate at particular frequencies and bandwidths. Either solution is practical and efficient for multi-band TSV_As transmitting at separate frequencies.

C. TSV_A Without GND Plane

The bottom ground plane can be removed to extend the bandwidth of the TSV_A to ∼5 GHz. Increased bandwidth comes at the drawback of not having as many bands. For instance, between 40 GHz and 80 GHz, a 1 GHz bandwidth would enable 26 bands with a separation of 0.5 GHz between bands. For 5 GHz bandwidth, on the other hand, the number of bands falls to 7. S-parameters for a pair of TSV_A communicating at 5mm distance without the bottom ground plane are shown in Figure 8. The reflection coefficient is -30 dB and the transmission coefficient is -1.4 dB.

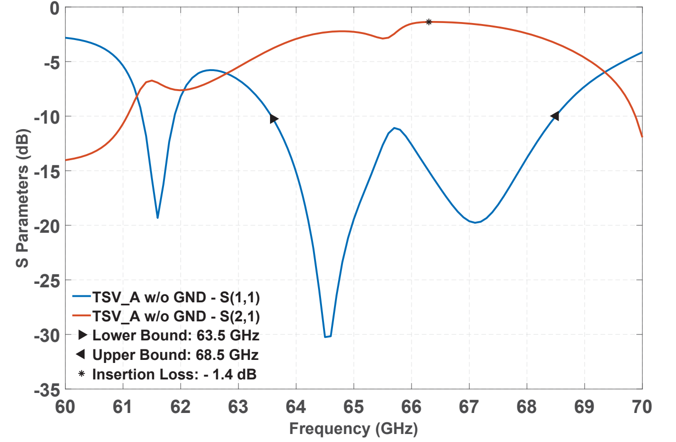

Fig. 8. S-parameters of TSV_A pair without bottom GND plane. (HFSS Simulated Results)

D. TSV_A Design Space Exploration

Design space exploration (DSE) is performed to provide general design guidelines for TSV_As. For generality, the geometry of the TSV is selected as a cylinder. For a specific technology or etching process, the geometry of the TSVs can be adjusted, for instance, into a circular cone with angled walls. The parameters in DSE are depicted in Figure 2. The TSV_A height is simulated from 500μm to 300μm, and the TSV_A radius is simulated from 120μm to 5μm. The manufacturing constraints of such TSVs with different radius and height need to be investigated, and if proven restraining, can be factored as design guidelines for a practical multi-band TSV_A implementation. In this work, manufacturing limitations are considered very broadly, not specific to one solution but a broader range of available geometries from literature.

TABLE I. TSV_A Design Space Exploration (@60 GHz)

Parameters	Design Range	TSV_A Change
TSV Height	300-500 μm	⟶ Carrier Frequency: ±15 GHz
TSV Radius	5-120 μm	⟶ Carrier Frequency: ±5 GHz
Disc Radius	5-120 μm	⟶ Return Loss: ±10 dB
Si Gap	1-15 μm	⟶ Return Loss: ±10 dB

The results of these multitude of experiments are shown in Table I and presented as follows. It is observed, in design space exploration, that the TSV_A height shifts the carrier frequency between the 50 GHz and 75 GHz bands, and the increasing TSV_A radius adds an additional 5 GHz range. Shorter TSV_As with a smaller radius operate at higher frequencies. Smaller Si gap and larger disc radius improve the reflection coeff. up to 10 dB. The disc radius and Si gap are simulated from 120μm to 5μm and 15μm to 1μm, respectively. Each design parameter changes particular characteristics of the

wireless channel at varied magnitudes, making the TSV_A a highly configurable wireless interconnect.

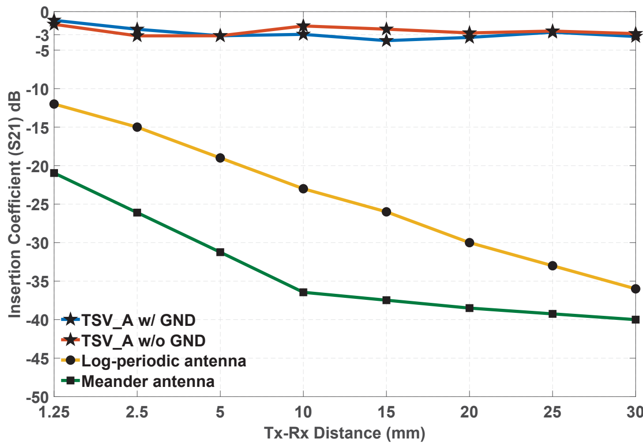

Fig. 9. Transmission coefficient (S21) versus distance for TSV_A, log-periodic [38] and meander [26] antennas. (HFSS Simulated Results)

E. Path Loss Analysis

Path loss is a major component in the characterization of transmission distance and power consumption, and represents the reduction of the input power as the EM field propagates through the substrate. Transmission coefficient (S21) represents the power received at the second TSV_A relative to the power input to the first TSV_A (higher is better). Path loss analysis is performed for the TSV_A with and without the bottom ground plane and compared against the planar log-periodic [4, 38] and meander [25, 26] antenna. The results of the evaluation are shown in Figure 9. The two TSV_As (Tx and Rx) are placed at increasing distances (1.25mm–30mm) from each other and the transmission coefficient (S21) is recorded from the HFSS FEM simulations. The TSV_A has an almost constant and very low *-3 dB* path loss due to the undoped silicon substrate layer acting as a wireless waveguide for the signal. These path loss properties hold true with or without the bottom ground plane, thus the bottom ground plane being marked optional. The planar log-periodic and meander antennas suffer from exponential increase in path loss (up to -40 dB for the meander and up to -35 dB for the log-periodic antennas) due to the surface-propagation of the EM field.

The addition of multi-band support of the TSV_A compared to the other antennas sacrifices bandwidth. TSV_As with increased bandwidth can be implemented by not including the bottom ground plane. The TSV_A without the bottom ground plane has a very similar path loss of -3 dB. The TSV_A without the bottom ground plane has an increased bandwidth of $\sim$5 GHz compared to the TSV_As with the bottom ground plane added. Improved path loss leads to several benefits, including: 1) The removal of low-noise amplifiers (LNAs), 2) low and constant power consumption, and, 3) increased TSV_A position flexibility during design-time.

F. TSV_A Interference from TSV

In Figure 10, two TSV_As are placed on the same board at a distance of 6mm. Multiple rows of TSVs are added between the TSV_As to quantify the interference caused from other TSVs in the system. Multiple structures are evaluated including a sweep of 1 to 4 TSV rows, and additionally 50 other structures with randomly placed TSVs on the board, as shown in Figure 11. Reflection coefficient (S11) and transmission coefficient (21) for all obstructions are shown in Table II. The resonant frequency is 60 GHz. All TSVs have a radius of 20μm and are equally spaced at 225μm. The reflection and transmission coefficients of the 50 randomized placements are averaged together. Without any obstruction, the TSV_As has a reflection coeff. of -16 dB and transmission coeff. of -2.2 dB. With 3 or 4 TSV rows of obstruction, the minimum reflection and transmission coeff. are -8.5 dB and -17 dB, respectively.

The average reflection and transmission coeff. of the TSV_As with the randomized TSV obstructions are -15.5 dB and -6.6 dB, respectively. TSV_A is shown to operate with additional TSVs in the silicon substrate layer, and even in the worst-case scenario it performs better than the planar log-periodic [4, 38] and meander [25, 26] antennas, at -20 dB to -30 dB at 6mm distance, without any interference. For optimal signal performance, the substrate layer can be dedicated only to the TSV_As for RF communication. If the silicon substrate layer cannot be dedicated to the TSV_As, guidelines can be developed for floorplanning to minimize interference between TSV_As and typical TSVs.

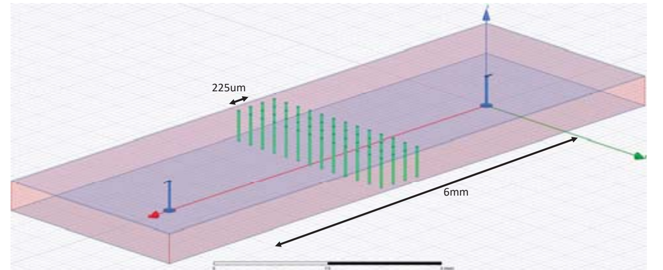

Fig. 10. TSV_A pair obstructed by 4 rows of TSVs. (Scale 0-3mm, HFSS Simulated Results)

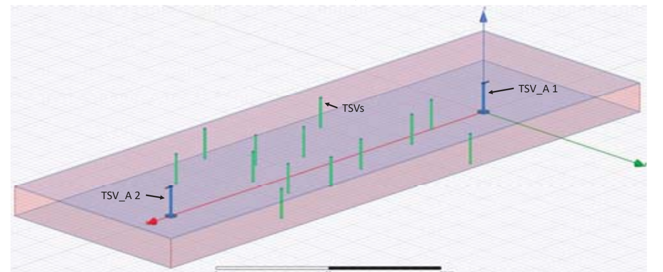

Fig. 11. TSV_A pair obstructed by randomly placed TSVs. (Scale 0-3mm, HFSS Simulated Results)

G. PCB Prototype [12] of TSV_A Design (PCB TSV_A)

The PCB measurement results in [12] are used to characterize the TSV_As, and to prove the fidelity of HFSS results for TSV_A implementations in IC integration. The

TABLE II. TSV impact on TSV_A performance.

Obstruction	Reflection Coeff. (S11)	Transmission Coeff. (S21)
None	-16 dB	-2.2 dB
1 Row TSV	-12 dB	-7 dB
2 Row TSV	-12 dB	-12 dB
3 Row TSV	-8.5 dB	-16 dB
4 Row TSV	-8.5 dB	-17 dB
Random	-15.5 dB	-6.6 dB

PCB prototypes use the Rogers RO4003C material with a dielectric constant ε_r of 3.55 and a dielectric tangent loss of 2.7×10^{-3}, high resistivity (HR) silicon for 3D ICs has up to 10 $\mathrm{k\Omega \cdot cm}$ which corresponds to a conductivity of $1 \times 10^{-2}\ \mathrm{S\,m^{-1}}$. Tangent loss of HR silicon is calculated as [2]:

$$tan\ \delta = \frac{\sigma}{\omega * \epsilon}, \tag{2}$$

where σ is the electrical conductivity of the medium, ω is the angular frequency, and ϵ represents permittivity of the medium.

Considering a resistivity of 3 $\mathrm{k\Omega \cdot cm}$ for silicon (ε_r of 11.7) in 3D ICs, the tangent loss at 20 GHz is calculated as 2.6×10^{-3}, approximately the same as the tangent loss of the Rogers RO4003C material. This similarity of tangent loss value is the rationale behind evaluating the TSV_A PCB prototype as a surrogate for the (prohibitively costly) 3D IC TSV_As.

Fig. 12. Photo of all fabricated PCB structures next to a US quarter. Each square in the background has 5mm sides.

The PCB prototype board housing the TSV_A structures at 400mil and 800mil distance is shown in Figure 12. Measured and simulated results of the PCB TSV_A prototypes are juxtaposed in Figure 13 and 14. There are multiple major *measured* resonant frequencies as shown in Figure 13. These resonant frequencies are 24, 29 and 35 GHz. The reflection coeff. for these frequencies is between -9 and -15 dB and the transmission coeff. is -6 to -9 dB. The simulated results match the measured results quite closely (within 2–5 dB) and all resonant frequencies are accounted for in the HFSS results. Note that the transmission coefficient includes the loss from the CPW feed, therefore actual loss from the TSV_A alone is even lower.

For the TSV_As placed at a further distance of 800mil, there are still multiple resonant frequencies, as shown in Figure 14. These resonant frequencies are 29, 34 and 37 GHz. Transmission coeff. is consistently less than -10 dB for each of the major resonant frequencies. The simulated results match the measured results, although a little less accurately, but within 2 to 5 dB accuracy at the resonant frequencies. Vector Network Analyzer measurements from [12] support the

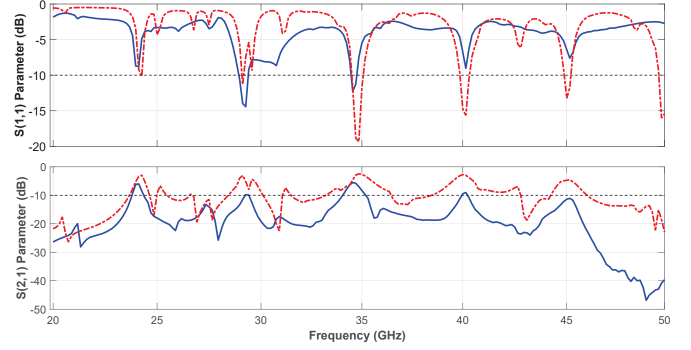

Fig. 13. Measured (blue) vs simulated (red) TSV_As at 400mil distance.

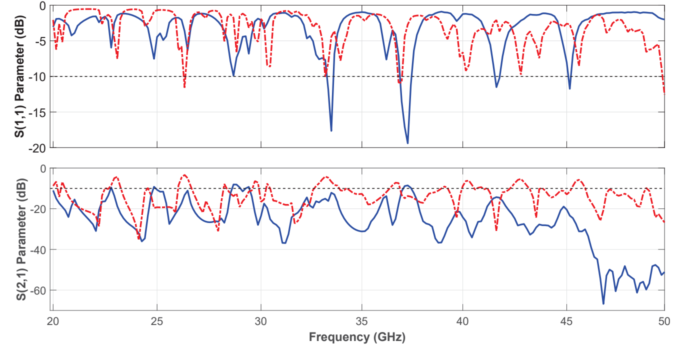

Fig. 14. Measured (blue) vs simulated (red) TSV_As at 800mil distance.

conclusion that: i) The HFSS simulations of TSV_As have high fidelity, and ii) the proposed TSV_As support multiple resonant frequencies, with transmission coeff. below -10 dB at distances that are verified in measurements to 20mm.

V. WNoC Performance Analysis of TSV_As

Cycle-accurate network simulations are performed to measure performance improvement, and estimate the power consumption of the proposed multi-band WNoC with TSV_As. Details about the WNoC simulator, traffic patterns, and routing algorithm are presented in Section V-A. To improve the network coverage of the TSV_As, a heuristic antenna placement algorithm is proposed in Section V-B. The algorithm is contrasted with a Monte Carlo uniform distribution analysis to quantify the TSV_A placement WNoC performance. WNoC performance evaluations of throughput, energy per flit, latency, and energy-delay product for multiple configurations are shown in Section V-C. The performance impact of TSV_A failure on a WNoC with 4 wireless bands is evaluated in Section V-D. The analyses of NoC area and the impact of technology scaling are detailed in Section V-E.

A. Simulation Setup

A cycle-accurate SystemC network simulator is used to perform the WNoC with multi-band performance evaluation. Multiple design choices, including mesh size and buffering, are shown in Table III. The mesh size arbitrarily chosen for this

evaluation is 12×12 (total 144 PEs), and the total number of wireless antennas is 64 TSV_As. Multiple band configurations are evaluated, ranging from 1 single band of 64 TSV_As on the WNoC to 8 separate bands of 8 TSV_As. The packet size is 10 flits and the flit size is 32 bits. Area and power estimations are performed utilizing the latest version of DSENT [39]. The energy per bit and area values of the wireless transceiver are obtained from Yu et al. [20, 21].

A 12x12 mesh is arbitrarily chosen as a baseline NoC to guarantee both dimensions equal as opposed to 128 PEs which would not allow an even distribution of the PEs. Larger NoC evaluation (256+ PEs) is considered too large as the primary evaluation setup. Although, larger NoC sizes would provide additional insight on the benefits of multi-band, the current baseline NoC size is selected due to the higher possibility for adoption in industry compared to larger NoCs. In addition, alternative NoC designs are not considered as the aim is to provide a clear and concise WNoC performance evaluation of the benefits of multi-band support alone.

TABLE III. Wireless NoC Parameters

Parameter	Design
Mesh size	12x12
Total # of PEs	144 PEs
# of Virtual Channels	4 VCs
# of Router I/O Buffers	4 (flits)
# of TSV_As	64
# of TSV_A Buffers	10 (flits)
Flit Size	32 bits
Packet Size	10 flits

1) WNoC Traffic Patterns Overview: Five traffic patterns are used to analyze the WNoC: 1) uniform random, 2) bit transpose, 3) bit reversal, 4) shuffle, and 5) butterfly. The main focus of this WNoC analysis is to provide a thorough investigation of *network* performance utilizing TSV_As, focusing solely on the packet-transfer aspect, so the synthetic traffic is appropriate (and preferred). Real application workloads such as Splash2 and Parsec3 benchmarks [40, 41] have low utilization rate of the NoC and do not allow for thorough network analysis.

2) WNoC Routing Algorithm: The routing algorithm utilized in the WNoC is a simplistic shortest path route used in prior WNoC studies [17, 42]. The algorithm combines the standard deterministic XY routing and wireless transmission. In particular, the distance between the source and the destination through a wireless link is compared to the distance of a conventional wired link between the source/destination pair before committing to either link. Packet routing through the wired links is carried out with a deterministic XY-dimension order routing algorithm. Deadlock-freedom is achieved by using multiple virtual channels (VCs). A token-passing arbitration mechanism is used between the wireless nodes operating in the same frequency band. The token dictates which TSV_A can transmit at that particular cycle. This selective approach in the usage of the wireless links avoids creating bottlenecks in the network. After the placement of the TSV_As each node can be either TSV_A-equipped or not, therefore the router is checked

Algorithm 1 Multi-Band Antenna Placement for WNoC.

Input:

Number of wireless bands W, Number of TSV_As per wireless band,

t: current temperature for SA,
t_{final}: final temperature for SA,
i_{total}: number of iterations at each temperature for SA.
f: Cost function,
α: Temperature reduction function,

Output:

A two dimensional array representing TSV_As on a WNoC with values representing the TSV_A position and the wireless band.

```
1:  for each Band ∈ W do
2:      Generate initial mapping M_0
        {Start annealing...}
3:      while t > t_final do
4:          for i = 1 to i_total do
5:              Generate new mapping M
6:              δ = f(M) − f(M_0)
7:              if δ < 0 then
8:                  M_0 = M
9:              else
10:                 Generate random number x from 0 to 1
11:                 if x < exp(−δ/t) then
12:                     M_0 = M
13:                 end if
14:             end if
15:         end for
16:         t = α(t)
17:     end while
18:     Return M_0
19: end for
```

if it can wireless transmit the packet and if the receiving TSV_A is closer than the wired distance utilizing XY routing. The algorithm only checks for TSV_As that are in the same frequency band as the current TSV_A-equipped router. Band hopping during transmission, i.e. one packet originating in one band but switching bands through the wired mesh routing, is permitted in the routing algorithm. If the token is not currently assigned to the current TSV_A, the packet is placed in a buffer for transmission. If there is no space in the buffer assigned to the wireless link for the head flit of the packet to wait for the token, then the packet is routed through the wired mesh.

B. WNoC Multi-Band Placement

As discussed in Section IV-A, the TSV_A has multi-band properties tied to the parameter configuration of the TSV acting as the main radiating element. Other antenna designs show multi-band properties [43] as well, but their concurrency dictates more complex modulation logic for each band. Increased modulation logic for each band on one antenna leads to larger area and power consumption [20]. The TSV_A varies

wireless bands based on simple physical properties (such as TSV radius), decreasing the overall complexity of modulation for each antenna, in addition to three orders of reduction in antenna size (µm size TSV_As vs mm-long antennae in literature). Furthermore, more complex modulation (as opposed to the basic on-off keying) can be applied to the TSV_As for an additional increase in the number of bands. Antenna placement is critical in ensuring the highest wireless throughput for the WNoC with TSV_As. Existing multi-band antennas in literature (which have multiple resonant frequencies) do not consider wireless coverage (if the signal from each antenna can reach the entire area of the chip) because their modulation logic handles all traffic from all bands. To this end, this is the first paper to propose a TSV_A placement algorithm for multi-band WNoCs to improve network throughput and latency.

1) Multi-Band Placement Algorithm: The main objective of Algorithm 1 is to minimize the aggregate hop count of the NoC by introducing shortcut links in the network through the TSV_As. The solution space for antenna placement grows exponentially with mesh size, therefore Algorithm 1 is based on simulated annealing (SA) [44]. The algorithm presented in Algorithm 1 is heuristic in nature and is not the optimal implementation in terms of execution time. Further improvements can be made to the algorithm to improve parallelism and decrease execution time. The input to the algorithm takes into account the mesh dimensions, the number of wireless bands, and the number of TSV_As for each band. The first step of the algorithm is to calculate the aggregate hop count without TSV_As, which is calculated as the sum of all hops for all source and destination pairs utilizing XY routing. After the cost function $totalDist$ is calculated, a random placement M_0 of all TSV_As in a band is performed. Simulated annealing (line 3) randomly swaps TSV_As with their nearest neighbors for i amount of iterations and generates a new mapping M (line 5). The cost function is re-calculated (line 6), if it is smaller than the current $totalDist$ the current placement M of the TSV_A replaces M_0 (lines 6–8). If the random swap affected $totalDist$ negatively, there is a possibility (lines 9–12) that the mapping M_0 will still be replaced by m (line 12). The updated $totalDist$ and mapping are then used as the new reference for other swaps. Additional TSV_A swaps are performed for the total number of iterations i, afterwards t is decremented by 5% and the procedure is repeated until t_{final} (line 3). This process is completed for all wireless bands (line 1) and the $totalDist$ is updated throughout with the new added wireless shortcut links. The final result of the algorithm is a placement of all TSV_As from all available wireless bands to globally minimize the aggregate hop count of the WNoC.

2) Multi-Band Monte Carlo Analysis: Monte Carlo uniform distribution analysis is performed to evaluate the efficacy of Algorithm 1. A thousand (1,000) different random TSV_A mappings for *each* packet injection rate are compared to the WNoC with TSV_As placed using Algorithm 1. The number of bands is kept constant at 4 frequency bands, and each band is equipped with 16 TSV_As. Performance is measured as average latency on a 12×12 WNoC, utilizing uniform random traffic, all other parameters are described in Table III. The Algorithm performs consistently under the mean for the average delay and has the added benefit of being adaptable for various topologies and larger WNoCs which may require an excessive sweep of Monte Carlo simulations.

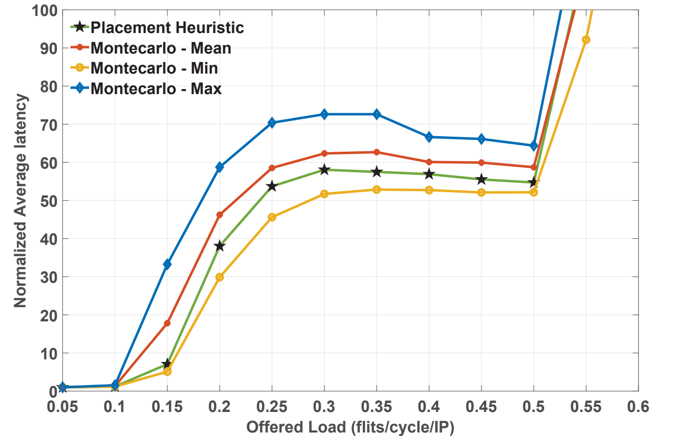

Fig. 15. Monte Carlo analysis of latency in a WNoC.

C. WNoC Performance Evaluation

Simulations results of the multiple WNoC configurations under different synthetic traffic patterns are shown in Figure 16. The performance metrics evaluated are:

1) Throughput,
2) Average energy per flit,
3) Normalized average latency, and,
4) Energy-delay per flit.

The results shown are focused on the performance at network saturation for each WNoC configuration, a norm in NoC literature. In order to identify the network saturation point for each network traffic pattern and configuration, the packet injection rate is analyzed from 0.05 up to 0.9 flits/cycle/IP. For instance, network saturation of WNoC with 4 wireless bands for uniform random traffic pattern occurs at ∼0.5 flits/cycle/IP. Additional details regarding the WNoC configuration, including VC count and packet size, are shown in Table III.

Throughput: Throughput results are shown in Figure 16(a). Across all traffic patterns and multiple wireless bands, network throughput improves considerably. The improvement is up to ∼52% in the *uniform random* traffic pattern compared to the flat mesh topology. Each traffic pattern favors a different WNoC configuration, the *uniform random* traffic pattern clearly favors as many wireless bands as possible, which in turn increase the total number of flits-in-flight. Because the *uniform random* traffic pattern does not have a specific source-destination mathematical model (as opposed to the other patterns), throughput improvement of ∼52% from the flat mesh and ∼29% from the single band WNoC is directly correlated to the increase in wireless channels/bands. Similar behavior is observed with the *bitreversal* and *shuffle* traffic pattern, up to ∼33% compared to the single band WNoC. The WNoC running the *transpose* traffic pattern has the highest throughput of ∼35% with 4 bands as opposed to other configurations. Increased the number of bands, while

increasing the flits in flight, also decreases overall coverage. Therefore, some locations might be reachable only through partial wireless and wired traversals, which in turn lowers the total throughput of the network. The *butterfly* traffic pattern does not utilize the benefits of added bands, as throughput improvement is constant at ∼6% with an increasing number of wireless channels.

Latency: Network latency evaluation is shown in Figure 16(b). Similar to throughput, latency is improved across the board, up to ∼38% when compared against the flat mesh topology. The *bitreversal* and *shuffle* traffic patterns display an increase in latency with an increasing number of wireless bands. This is attributed to the additional hops necessary reach the destination in case the destination node is not in close proximity to the TSV_A. The ratio of TSV_A to router for any particular band is decreased with the addition of bands and additional hops are required to complete the transmission. These additional hops happen in the wired mesh because the distance in hops to the destination is fewer than the wireless link choice. In the case of the *uniform random* traffic pattern, latency is improved up to ∼10% with the addition of multi-band support. The largest improvement in latency comes from the *butterfly* traffic patterns, with an improvement of up to ∼14% in latency. WNoC running the *transpose* traffic pattern has an improvement in latency up to ∼7% with added multi-band support.

Energy per flit: The energy per flit is defined as the average energy consumed to transmit a single flit through the network. Energy per flit evaluation of multiple WNoC configurations is shown in Figure 16(c). A WNoC offering a higher performance is expected to have a lower saturation energy per flit. Energy estimations are performed utilizing the latest version of DSENT using the 32nm technology node. The energy for a wireless transfer is 1.2 pJ/bit based on the transceiver proposed in [20, 21] using the 65nm technology node. No power scaling for the OOK transceiver has been performed. According to Figure 16(c), there is a decrease of ∼28% in energy per flit compared to the flat mesh topology. This is excepted when considering the increase in network throughput of ∼52% and decrease in network latency of ∼38%. In the case of the *uniform random* traffic pattern, the increase in energy per flit from 1 band to 8 bands is ∼10%. The *transpose* and *butterfly* traffic patterns have an improvement in energy consumption with 4 wireless bands, up to ∼20% and ∼5%, respectively. The *bitreversal* and *shuffle* traffic patterns show decreased energy per flit up to ∼30% on 8 bands compared to the single band. These traffic pattern offers a higher load to the diagonal across the WNoC, the wireless interconnect is used more often and more transactions are completed, therefore a decrease in energy per flit.

Energy-delay product: Energy-delay product evaluation is shown in Figure 16(d). This performance metric is especially useful because network latency and energy per flit are both taken into account, therefore characterizing the improvement in network performance considering the added energy consumption. All traffic patterns display an improvement in EDP when contrasted against the flat mesh. This is partly attributed to the improvement in latency across the board for all traffic patterns. An average improvement of ∼35% and a maximum of ∼50% in EDP are obtained through the WNoC multi-band configurations. The *uniform random* traffic pattern has an EDP improvement of ∼50% in the single band configuration, Multi-

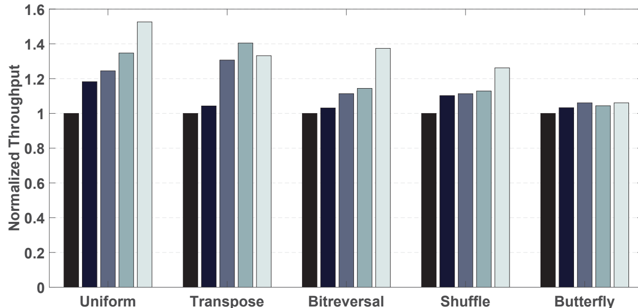

(a) Normalized saturation throughput.

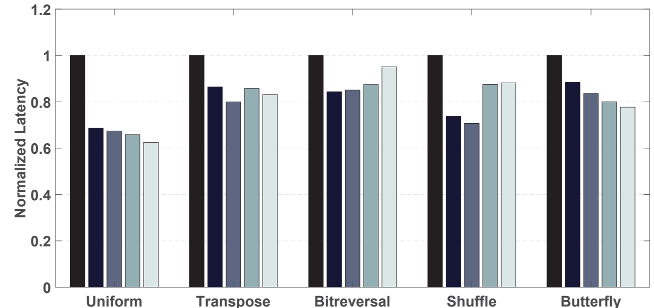

(b) Normalized average latency before saturation.

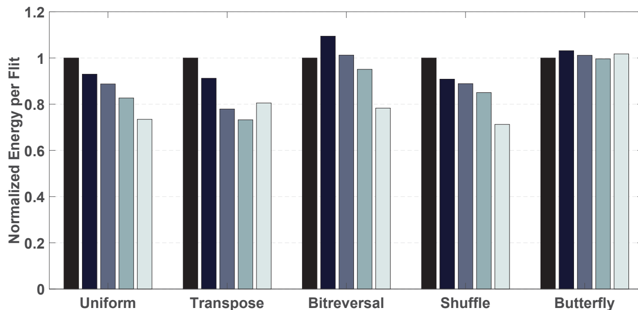

(c) Normalized Average energy/flit at saturation.

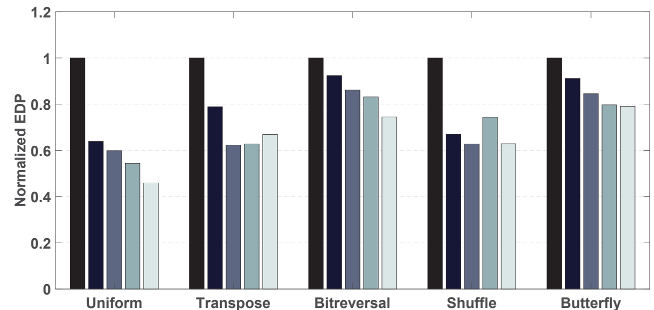

(d) Normalized energy-delay/flit at saturation.

Wired NoC mesh   WNoC - 1 Band   WNoC - 2 Band   WNoC - 4 Band   WNoC - 8 Band

Fig. 16. Simulation results for varying synthetic traffic patterns.

ple bands also feature significant EDP improvement of ∼40% compared to the wired flat mesh. The *transpose* and *bitreversal* traffic patterns have an improvement in EDP with the increase of wireless bands. The *shuffle* traffic pattern improves EDP up to ∼7% when in 2-band and 8-band configuration, although EDP increases ∼10% in the 4-band configuration (compared to the single band configuration), which is still 6% better than flat-mesh. WNoC running the *butterfly* traffic pattern has an improvement in EDP up to ∼20% with the addition and increase of wireless bands. Although the *butterfly* traffic pattern only had ∼6% improvement in throughput and ∼3% in energy per flit, packet latency is improved drastically, therefore EDP is also improved considerably.

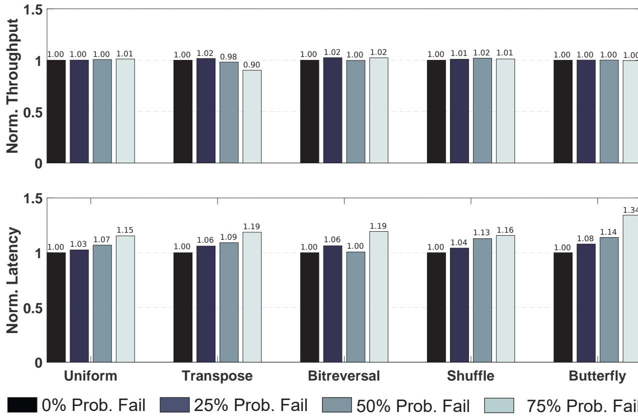

Fig. 17. WNoC - 4 Band performance impact of failure rate.

D. Performance Evaluation in Case of Failure

In Figure 17, the performance impact of TSV_A failure on a WNoC with 4 wireless bands is evaluated. Fault detection and the mitigation process have additional overhead not included in this work. Instead, this evaluation focuses on the performance impact in case of a failure with a probability. Fault-tolerant techniques in literature that provide effective fault-tolerant routing schemes include [45–47]. These schemes can be implemented into WNoC with TSV_As and multi-band to improve performance and reliability, and to more accurately reflect the design overhead.

Failure analysis is performed assuming that for each wireless transmission during the simulation runtime, there is a failure probability ranging from 0% to 75%, similar to other work in reliability [45, 47]. If the transmission fails then the packet is re-routed through the wired mesh until it reaches its destination or another router equipped with a TSV_A. Throughput and latency are measured across multiple synthetic traffic patterns and 4 probability rates.

Throughput: Across most traffic patterns and multiple failure rates, network throughput remains constant. This can be attributed to the balanced network utilization achieved by re-routing packets through the wired mesh. WNoC running the *transpose* traffic pattern has a lower throughput of ∼10% with a TSV_A failure rate of 75% as opposed to other failure rates. The *transpose* traffic pattern offers a higher load to the diagonal across the WNoC causing a bottleneck on the wired mesh due to the high wireless demand and high failure rate.

Latency: Across most traffic patterns and multiple failure rates, network latency increases considerably. The increase in latency is up to ∼34% in the *butterfly* traffic pattern compared to the 0% failure rate. Latency increase is linear with the increase of failure, up to ∼15% in the *uniform random* traffic pattern. This increase in latency is attributed to the decrease in usage of the wireless interconnect provided by the addition of TSV_As in the WNoC.

All other bands display similar performance degradation, although due to the re-routing of packets towards the wired mesh in case of failure, the system never fully fails and is able to complete the simulation.

E. Area and Technology Scaling

Area and technology scaling analysis are performed to evaluate the impact of future scaling trends on the WNoC with TSV_As. The area overheads for the router, antennas, and transceiver are shown for multiple technology nodes in Figure 18. These numbers account for individual routers, antennas, and transceivers. The antennas measured are the planar log-periodic [4], meander [25] and TSV_A. In the case of multiple wireless bands, the area of the largest TSV_A is selected. The radius of the TSV_A is increased by 10μm for each additional band. The area for the TSV_A has been quadrupled to account for keep-out-zones and pitch requirements. The area of the single band TSV_A is 1600 μm^2, the area of the largest TSV_A in the 4-band configuration is 2.56×10^4 μm^2.

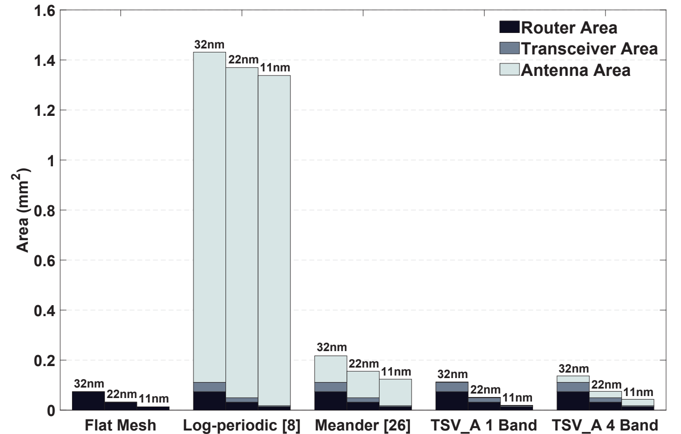

Fig. 18. Area estimation for multiple technology nodes.

In contrast, the area for the log-periodic antenna is 1.32×10^6 μm^2, and the area of the meander antenna is 1.06×10^5 μm^2. The proposed single-band TSV_A offers 99.88% and 98.49% area reduction compared to the planar log-periodic and meander antennas, respectively.

The original design for the transceiver proposed in [20, 21] is in the 65nm technology node. Area scaling from 65nm to smaller technology nodes is performed following standard CMOS scaling equations described in [48]. In the case of the TSV_As, the largest impact in network area is attributed to the router logic/buffering and the OOK transceiver for the wireless

interconnects. On the other hand, the meander and planar log-periodic antennas are exponentially larger than the TSV_A solution. The area overheads for both router and transceiver decrease with technology scaling. The TSV_A area depends on the number of bands and the carrier frequency.

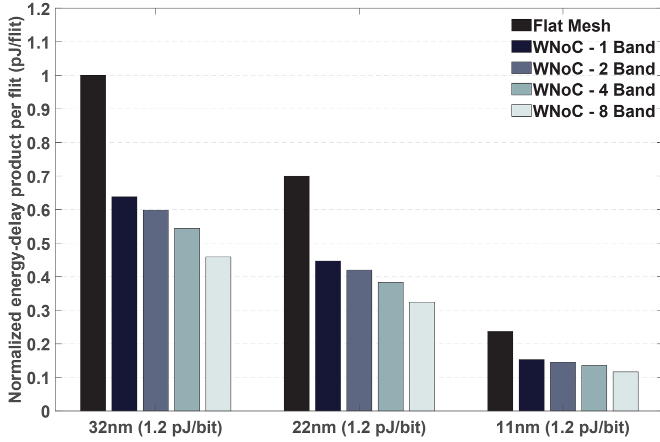

Fig. 19. Energy-delay product for multiple technology nodes for uniform traffic with 1.2 pJ/bit TSV_As.

The normalized energy-delay product per flit for WNoC on a *uniform random* traffic pattern at multiple technology nodes is shown in Figure 19. Significant EDP improvement of $\sim$50% can be achieved with the addition of TSV_As in the flat mesh. Additional bands show an improvement of $\sim$40% over the flat mesh topology. Technology node scaling does not impact the benefits in EDP of up to $\sim$50%, the EDP improvement is sustained in both the 22nm and 11nm technology nodes.

VI. Conclusions and Future Work

This work proposes a novel communication infrastructure, utilizing TSVs for on-chip wireless communication. FEM and cycle-accurate system simulations are performed to 1) validate the operation of the TSV antenna (TSV_A), and 2) provide Network-on-Chip performance evaluations. HFSS results demonstrate that the TSV_A can be configured to operate in multiple frequency bands, allowing for Wireless NoCs with multiple wireless channels or wireless intercell communication in reconfigurable metasurfaces at practically no cost in area and energy consumption.

A placement algorithm is proposed to place TSV_As on a WNoC, and system-level evaluation is performed to measure the performance improvement. Results show that each workload has an increase in throughput and decrease in latency at various WNoC band configuration. Throughput improvement is on average 23% (increasing the number of bands from single band) and can reach as high as $\sim$34%. Latency improvements are $\sim$7% on average and can reach $\sim$13% in specific workloads. Energy benefits are $\sim$21% on average and can reach $\sim$29% in specific workloads. Energy-delay product improvements are $\sim$34% on average and can reach $\sim$50% in specific workloads. The highly configurable nature of TSV_As enables different configurations which are tailored to specific workloads or design choices.

Future work on TSV_As will focus on improving transmission bandwidth even further while maintaining ease of fabrication and implementation. The application of TSV_A in metasurfaces, mentioned in Section I-A, would benefit from such improved transmission bandwidth. The analysis in future work will include TSV_A for intercell wireless communication in reconfigurable metasurfaces. System integration rules of TSV_As, to support desired robustness as described in Section III-A, will be studied in the future.

References

[1] K. Kim and K. K. O, “Integrated dipole antennas on silicon substrates for intra-chip communication,” in *IEEE Antennas and Propagation Society International Symposium*, vol. 3, pp. 1582–1585, July 1999.

[2] K. K. O, K. Kim, B. A. Floyd, J. L. Mehta, H. Yoon, C. M. Hung, D. Bravo, T. O. Dickson, X. Guo, R. Li, N. Trichy, J. Caserta, W. R. Bomstad, J. Branch, D. J. Yang, J. Bohorquez, E. Seok, L. Gao, A. Sugavanam, J. J. Lin, J. Chen, and J. E. Brewer, “On-chip antennas in silicon ics and their application,” *IEEE Transactions on Electron Devices*, vol. 52, pp. 1312–1323, July 2005.

[3] K. K. O, K. Kim, B. Floyd, J. Mehta, H. Yoon, C. Hung, D. Bravo, T. Dickson, X. Guo, R. Li, N. Trichy, J. Caserta, W. Bomstad, J. Branch, D. Yang, J. Bohorquez, J. Chen, E. Seok, L. Gao, A. Sugavanam, J. Lin, S. Yu, C. Cao, M. Hwang, Y. Ding, S.-H. Hwang, H. Wu, N. Zhang, and J. E. Brewer, “The feasibility of on-chip interconnection using antennas,” in *Proceedings of the IEEE/ACM International Conference on Computer-Aided Design (ICCAD)*, pp. 979–984, November 2005.

[4] H. Mondal, S. Gade, M. Shamim, S. Deb, and A. Ganguly, “Interference-aware wireless Network-on-Chip architecture using directional antennas,” *IEEE Transactions on Multi-Scale Computing Systems*, vol. PP, pp. 1–1, July 2016.

[5] A. Mineo, M. Palesi, G. Ascia, and V. Catania, “Exploiting antenna directivity in wireless NoC architectures,” *Elsevier Microprocessors and Microsystems*, vol. 43, pp. 59 – 66, 2016.

[6] F. Liu, A. Pitilakis, M. S. Mirmoosa, O. Tsilipakos, X. Wang, A. C. Tasolamprou, S. Abadal, A. Cabellos-Aparicio, E. Alarcón, C. Liaskos, N. V. Kantartzis, M. Kafesaki, E. N. Economou, C. M. Soukoulis, and S. Tretyakov, “Programmable metasurfaces: State of the art and prospects,” in *2018 IEEE International Symposium on Circuits and Systems (ISCAS)*, pp. 1–5, May 2018.

[7] S. E. Hosseininejad, K. Rouhi, M. Neshat, A. Cabellos-Aparicio, S. Abadal, and E. Alarcón, “Digital metasurface based on graphene: An application to beam steering in terahertz plasmonic antennas,” *IEEE Transactions on Nanotechnology*, vol. 18, pp. 734–746, 2019.

[8] A. C. Tasolamprou, M. S. Mirmoosa, O. Tsilipakos, A. Pitilakis, F. Liu, S. Abadal, A. Cabellos-Aparicio, E. Alarcón, C. Liaskos, N. V. Kantartzis, S. Tretyakov, M. Kafesaki, E. N. Economou, and C. M. Soukoulis, “Intercell wireless communication in software-defined metasurfaces,” in *2018 IEEE International Symposium on Circuits and Systems (ISCAS)*, pp. 1–5, May 2018.

[9] A. C. Tasolamprou, A. Pitilakis, S. Abadal, O. Tsilipakos, X. Timoneda, H. Taghvaee, M. Sajjad Mirmoosa, F. Liu, C. Liaskos, A. Tsioliaridou, S. Ioannidis, N. V. Kantartzis, D. Manessis, J. Georgiou, A. Cabellos-Aparicio, E. Alarcón, A. Pitsillides, I. F. Akyildiz, S. A. Tretyakov, E. N. Economou, M. Kafesaki, and C. M. Soukoulis, “Exploration of intercell wireless millimeter-wave communication in the landscape of intelligent metasurfaces,” *IEEE Access*, vol. 7, pp. 122931–122948, 2019.

[10] H. Taghvaee, S. Abadal, J. Georgiou, A. Cabellos-Aparicio, and E. Alarcón, “Fault tolerance in programmable metasurfaces: The beam steering case,” in *2019 IEEE International Symposium on Circuits and Systems (ISCAS)*, pp. 1–5, May 2019.

[11] V. Pano, I. Tekin, Y. Liu, K. Dandekar, and B. Taskin, “In-package wireless communication with tsv-based antenna,” in *IEEE International Symposium on Circuits and Systems (ISCAS) Late Breaking News*, pp. 1–3, May 2019.

[12] V. Pano, I. Tekin, Y. Liu, K. Dandekar, and B. Taskin, “Tsv-based antenna for on-chip wireless communication,” in *IET Microwaves, Antennas and Propagation*, pp. 1–6, December 2019.

[13] B. A. Floyd, C.-M. Hung, and K. K. O, “Intra-chip wireless interconnect for clock distribution implemented with integrated antennas, receivers, and transmitters,” *IEEE Journal of Solid-State Circuits*, vol. 37, pp. 543–552, May 2002.

[14] J. J. Lin, H. T. Wu, Y. Su, L. Gao, A. Sugavanam, J. E. Brewer, and K. K. O, "Communication using antennas fabricated in silicon integrated circuits," *IEEE Journal of Solid-State Circuits*, vol. 42, pp. 1678–1687, August 2007.

[15] Y. Huang, W. Y. Yin, and Q. H. Liu, "Performance prediction of carbon nanotube bundle dipole antennas," *IEEE Transactions on Nanotechnology*, vol. 7, pp. 331–337, May 2008.

[16] P. P. Pande, A. Ganguly, K. Chang, and C. Teuscher, "Hybrid wireless network on chip: A new paradigm in multi-core design," in *Proceedings of the ACM International Workshop on Network on Chip Architectures (NoCArc)*, pp. 71–76, December 2009.

[17] A. Ganguly, K. Chang, S. Deb, P. P. Pande, B. Belzer, and C. Teuscher, "Scalable hybrid wireless Network-on-Chip architectures for multicore systems," *IEEE Transactions on Computers*, vol. 60, pp. 1485–1502, October 2011.

[18] X. Timoneda, S. Abadal, A. Cabellos-Aparicio, D. Manessis, J. Zhou, A. Franques, J. Torrellas, and E. Alarcón, "Millimeter-wave propagation within a computer chip package," in *2018 IEEE International Symposium on Circuits and Systems (ISCAS)*, pp. 1–5, May 2018.

[19] S. Abadal, A. Marruedo, A. Franques, H. Taghvaee, A. Cabellos-Aparicio, J. Zhou, J. Torrellas, and E. Alarcón, "Opportunistic beamforming in wireless network-on-chip," in *Proceedings of the IEEE International Symposium on Circuits and Systems (ISCAS)*, pp. 1–5, May 2019.

[20] X. Yu, J. Baylon, P. Wettin, D. Heo, P. P. Pande, and S. Mirabbasi, "Architecture and design of multichannel millimeter-wave wireless NoC," *IEEE Design Test*, vol. 31, pp. 19–28, December 2014.

[21] X. Yu, S. P. Sah, H. Rashtian, S. Mirabbasi, P. P. Pande, and D. Heo, "A 1.2-pj/bit 16-gb/s 60-ghz ook transmitter in 65-nm cmos for wireless Network-On-Chip," *IEEE Transactions on Microwave Theory and Techniques*, vol. 62, pp. 2357–2369, October 2014.

[22] M. F. Chang, V. P. Roychowdhury, L. Zhang, H. Shin, and Y. Qian, "Rf/wireless interconnect for inter- and intra-chip communications," *Proceedings of the IEEE*, vol. 89, pp. 456–466, April 2001.

[23] M. F. Chang, J. Cong, A. Kaplan, M. Naik, G. Reinman, E. Socher, and S. W. Tam, "CMP Network-on-Chip overlaid with multi-band rf-interconnect," in *Proceedings of the IEEE International Symposium on High Performance Computer Architecture (HPCA)*, pp. 191–202, February 2008.

[24] A. More and B. Taskin, "EM and circuit co-simulation of a reconfigurable hybrid wireless NoC on 2D ICs," in *Proceedings of the IEEE International Conference on Computer Design (ICCD)*, pp. 19–24, October 2011.

[25] H. Nakano, H. Tagami, A. Yoshizawa, and J. Yamauchi, "Shortening ratios of modified dipole antennas," *IEEE Transactions on Antennas and Propagation*, vol. 32, pp. 385–386, April 1984.

[26] M. Sun, Y. P. Zhang, G. X. Zheng, and W. Y. Yin, "Performance of intra-chip wireless interconnect using On-Chip antennas and UWB radios," *IEEE Transactions on Antennas and Propagation*, vol. 57, pp. 2756–2762, September 2009.

[27] S. Hwangbo, A. Rahimi, C. Kim, H. Yang, and Y. Yoon, "Through Glass Via (TGV) disc loaded monopole antennas for millimeter-wave wireless interposer communication," in *Proceedings of the IEEE Electronic Components and Technology Conference (ECTC)*, pp. 999–1004, May 2015.

[28] S. Hwangbo, A. B. Shorey, and Y. K. Yoon, "Millimeter-wave wireless intra-/inter chip communications in 3d integrated circuits using through glass via (TGV) disc-loaded patch antennas," in *Proceedings of the IEEE Electronic Components and Technology Conference (ECTC)*, pp. 2507–2512, May 2016.

[29] B. Kim, C. Sharbono, T. Ritzdorf, and D. Schmauch, "Factors affecting copper filling process within high aspect ratio deep vias for 3D chip stacking," in *Proceedings of the Electronic Components and Technology Conference (ECTC)*, pp. 838–843, June 2006.

[30] M. Puech, J. M. Thevenoud, J. M. Gruffat, N. Launay, N. Arnal, and P. Godinat, "Fabrication of 3D packaging TSV using DRIE," in *Proceedings of the Symposium on Design, Test, Integration and Packaging of MEMS/MOEMS (DTIP)*, pp. 109–114, April 2008.

[31] V. S. Rao, H. S. Wee, L. W. S. Vincent, L. H. Yu, L. Ebin, R. Nagarajan, C. T. Chong, X. Zhang, and P. Damaruganath, "TSV interposer fabrication for 3D IC packaging," in *Proceedings of the Electronics Packaging Technology Conference (EPTC)*, pp. 431–437, December 2009.

[32] J. H. Lau, "Evolution, challenge, and outlook of TSV, 3D IC integration and 3D silicon integration," in *Proceedings of the International Symposium on Advanced Packaging Materials (APM)*, pp. 462–488, October 2011.

[33] G. Katti, M. Stucchi, K. D. Meyer, and W. Dehaene, "Electrical modeling and characterization of through silicon via for three-dimensional ics," *IEEE Transactions on Electron Devices*, vol. 57, pp. 256–262, January 2010.

[34] J. Kim, J. S. Pak, J. Cho, E. Song, J. Cho, H. Kim, T. Song, J. Lee, H. Lee, K. Park, S. Yang, M. Suh, K. Byun, and J. Kim, "High-frequency scalable electrical model and analysis of a through silicon via (tsv)," *IEEE Transactions on Components, Packaging and Manufacturing Technology*, vol. 1, pp. 181–195, February 2011.

[35] B. A. Shenoi, *Introduction to Digital Signal Processing and Filter Design*. Wiley-Interscience, 2005.

[36] R. Abdaoui, M. Villegas, G. Baudoin, and A. Diet, "Microstrip band pass filter bank for 60 ghz uwb impulse radio multi band architectures," in *IEEE MTT-S International Microwave Workshop Series on Millimeter Wave Integration Technologies*, pp. 192–195, September 2011.

[37] S. XU, F. MENG, K. MA, and K. S. YEO, "State of the art in passive bandpass filter solutions for 60 ghz communications ghz communications," *ZTE COMMUNICATIONS*, vol. 14, no. S1, p. 1, 2016.

[38] A. Samaiyar, S. S. Ram, and S. Deb, "Millimeter-wave planar log periodic antenna for on-chip wireless interconnects," in *Proceedings of the European Conference on Antennas and Propagation (EuCAP)*, pp. 1007–1009, April 2014.

[39] C. Sun *et al.*, "DSENT - a tool connecting emerging photonics with electronics for opto-electronic networks-on-chip modeling," in *Proceedings of the IEEE/ACM International Symposium on Networks-on-Chip (NoCs)*, pp. 201–210, May 2012.

[40] S. C. Woo *et al.*, "The SPLASH-2 programs: characterization and methodological considerations," in *Proceedings of the ACM/IEEE International Symposium on Computer Architecture (ISCA)*, pp. 24–36, 1995.

[41] C. Bienia, *Benchmarking Modern Multiprocessors*. PhD thesis, Princeton University, January 2011.

[42] S. Deb, A. Ganguly, P. P. Pande, B. Belzer, and D. Heo, "Wireless NoC as interconnection backbone for multicore chips: Promises and challenges," *IEEE Journal on Emerging and Selected Topics in Circuits and Systems (JETCAS)*, vol. 2, pp. 228–239, June 2012.

[43] S. Deb, K. Chang, X. Yu, S. P. Sah, M. Cosic, A. Ganguly, P. P. Pande, B. Belzer, and D. Heo, "Design of an energy-efficient CMOS-Compatible NoC architecture with millimeter-wave wireless interconnects," *IEEE Transactions on Computers*, vol. 62, pp. 2382–2396, December 2013.

[44] S. Kirkpatrick, C. D. Gelatt, and M. P. Vecchi, "Optimization by simulated annealing," *Science*, vol. 220, no. 4598, pp. 671–680, 1983.

[45] A. Prodromou, A. Panteli, C. Nicopoulos, and Y. Sazeides, "NoCAlert: An On-Line and Real-Time fault detection mechanism for Network-on-Chip architectures," in *Proceedings of the IEEE/ACM International Symposium on Microarchitecture (MICRO)*, pp. 60–71, December 2012.

[46] C. Killian, C. Tanougast, F. Monteiro, and A. Dandache, "Smart reliable Network-on-Chip," *IEEE Transactions on Very Large Scale Integration Systems (TVLSI)*, vol. 22, pp. 242–255, February 2014.

[47] J. Liu, J. Harkin, Y. Li, and L. P. Maguire, "Fault-tolerant Networks-on-Chip routing with coarse and fine-grained look-ahead," *IEEE Transactions on Computer-Aided Design of Integrated Circuits and Systems (TCAD)*, vol. 35, pp. 260–273, February 2016.

[48] J. M. Rabaey, A. Chandrakasan, and B. Nikolic, *Digital Integrated Circuits*, p. 124. Prentice Hall Press, 3rd ed., 2008.

Vasil Pano Vasil Pano (S'16) received his B.S degree and PhD degrees from Drexel University, Philadelphia, PA, in Computer (B.S degree) and Electrical (PhD degree) Engineering in 2014 and 2019, respectively.

He is currently a Post Doctoral Resarcher at Drexel University, Philadelphia, PA. Dr. Pano has held an graduate intern position at Intel Corporation, Hillsboro, OR in their Data Center Group working towards a scalable network interconnect for exascale architectures. His research focuses on network-on-chips, wireless on-chip interconnects, and multi-die systems.

Ibrahim Tekin Ibrahim Tekin received the B.S and M.S degrees from the Department of Electrical and Electronics Engineering, Middle East Technical University, Ankara, Turkey, in 1990 and 1992, respectively. From 1993 to 1997, he was with the Department of Electrical Engineering, Ohio State University, Columbus, OH, USA, where he received the Ph.D. degree in 1997. From 1997 to 2000, he worked as a Researcher in Wireless Technology Lab of Bell Laboratories, Lucent Technologies.

Dr. Tekin is currently with the Electronics Engineering Program, Sabanci University, Istanbul. His research interests include RF and microwave circuit design, millimeter wave antennas and circuits. He is involved in various projects including Indoor positioning using GPS signals, 77 GHz LNA and antenna design, RFIC design for WLAN systems, antennas for full duplex systems. He is a Senior Member of IEEE Antennas and Propagation Society.

Isikcan Yilmaz Isikcan Yilmaz (S'16) received the B.S. and M.S degrees in computer engineering From Drexel University, Philadelphia, PA, USA in 2016 and 2018, respectively.

He has worked as an intern in topics such as memory technologies, cybersecurity, and embedded systems firmware development. His current research interests include embedded systems, thread scheduling, and cache technologies. Isikcan is currently a firmware developer for Apple Inc.

Yuqiao Liu Yuqiao Liu (S'11) received the B.S. degree in Physics and M.S. degree in Electrical Engineering from the Nanjing University of Science and Technology, Jiangsu, China, in 2004 and 2006, respectively. Currently he is a Ph.D. candidate in electrical and computer engineering in Drexel University, Philadelphia, PA, USA, From 2006 to 2010, he worked in ZTE corporation as an RF engineer who is responsible for designing RF front-end for 2G and 3G cellphones.

In 2009-2010, he led the research team designing the first NFC cellphone in China. He is the author and coauthor of several patents, and scientific papers in the field of reconfigurable antennas, wearable technologies, mmWave antennas and micro-doppler signature.

Kapil R. Dandekar Kapil R. Dandekar (S'95–M'01–SM'07) received the B.S. degree in electrical engineering from the University of Virginia, Charlottesville, VA, USA, in 1997, and the M.S. and Ph.D. degrees in electrical and computer engineering from the University of Texas at Austin, Austin, TX, USA, in 1998 and 2001, respectively.

In 1992, he was with the U.S. Naval Observatory, Washington, DC, USA. From 1993 to 1997, he was with the U.S. Naval Research Laboratory, Washington, DC, USA. In 2001, he joined the Electrical and Computer Engineering Department, Drexel University, Philadelphia, PA, USA, where he is currently a Professor in Electrical and Computer Engineering, the Director with the Drexel Wireless Systems Laboratory (DWSL), and an Associate Dean for Enrollment Management and Graduate Education. His current research interests include wireless, ultrasonic, and optical communications, reconfigurable antennas, and smart textiles.

Baris Taskin Baris Taskin (S'01-M'05-SM'12) received the B.S. degree in electrical and electronics engineering from Middle East Technical University, Ankara, Turkey, in 2000, and the M.S. and Ph.D. degrees in electrical engineering from the University of Pittsburgh, Pittsburgh, PA, in 2003 and 2005, respectively.

He joined the Electrical and Computer Engineering at Drexel University, Philadelphia, PA, in 2005, where currently he is a Professor. His research interests include electronic design automation (EDA) for VLSI, low-power circuits, resonant clocking, clock network synthesis, hardware/software design space exploration and network-on-chip (NoC) for chip multi-processors (CMPs).

Dr. Taskin is a recipient of a number of awards for his research and professional contributions, including the Association for Computing Machinery Special Interest Group on Design Automation (ACM SIGDA), A. Richard Newton Award in 2007, the National Science Foundation Faculty Early Career Development (NSF CAREER) Award in 2009, an ACM SIGDA Distinguished Service Award in 2012 and the Delaware Valley Young Electrical Engineer of the Year Award from the IEEE Philadelphia Section in 2013.